Structure
Article

Structural Basis of DNA Loop Recognition by Endonuclease V

Ida Rosnes,[1,2] Alexander D. Rowe,[1,2] Erik S. Vik,[1,2] Rune Johansen Forstrøm,[1] Ingrun Alseth,[1] Magnar Bjørås,[1,2] and Bjørn Dalhus[1,2,*]
[1]Department of Microbiology
[2]Department of Medical Biochemistry
Oslo University Hospital, Rikshospitalet, P.O. Box 4950, Nydalen, N-0424 Oslo, Norway
*Correspondence: bjorn.dalhus@medisin.uio.no
http://dx.doi.org/10.1016/j.str.2012.12.007

SUMMARY

The DNA repair enzyme endonuclease V (EndoV) recognizes and cleaves DNA at deaminated adenine lesions (hypoxanthine). In addition, EndoV cleaves DNA containing various helical distortions such as loops, hairpins, and flaps. To understand the molecular basis of EndoV's ability to recognize and incise DNA structures with helical distortions, we solved the crystal structure of *Thermotoga maritima* EndoV in complex with DNA containing a one-nucleotide loop. The structure shows that a strand-separating wedge is crucial for DNA loop recognition, with DNA strands separated precisely at the helical distortion. The additional nucleotide forming the loop rests on the surface of the wedge, while the normal adenine opposite the loop is flipped into a base recognition pocket. Our data show a different principle for DNA loop recognition and cleavage by EndoV, in which a coordinated action of a DNA-intercalating wedge and a base pocket accommodating a flipped normal base facilitate strand incision.

INTRODUCTION

Cellular DNA is constantly attacked by a number of exogenous and endogenous sources, threatening genomic integrity. To combat this problem, specific mechanisms for recognition and repair of various forms of DNA damage have evolved (Lindahl, 1993; Hoeijmakers, 2001, 2009; Friedberg et al., 2006). Endonuclease V (EndoV), an evolutionarily conserved DNA repair enzyme, is shown to play a significant role in the repair of deaminated adenine (hypoxanthine) in *Escherichia coli* (Demple and Linn, 1982; Yao et al., 1994; Yao and Kow, 1995; Weiss, 2008). This enzyme incises the DNA at the second phosphodiester bond 3′ to the lesion, leaving a 3′-OH and a 5′-phosphate termini (Yao et al., 1994). Additionally, EndoV recognizes a wide spectrum of other DNA substrates including xanthine, oxanine, uracil, base mismatches, abasic sites, insertion-deletion (ID) loops, hairpins, and pseudo-Y and flap structures, as well as forks and junctions (Yao and Kow, 1994, 1996, 1997; Yao et al., 1994; Huang et al., 2001; Hitchcock et al., 2004; Fladeby et al., 2012). Specifically, it has been shown that *E. coli* EndoV incises DNA substrates containing loops with two to 14 nucleotides. Cleavage takes place predominantly at the shorter strands' second phosphodiester bond 3′ of the loop. An additional incision at the first 3′ phosphodiester bond has also been observed, and two cleavage sites have also been identified on the DNA strand containing the loop (Yao and Kow, 1996).

Our previous crystal structure of *Thermotoga maritima* (*Tma*) EndoV in complex with hypoxanthine revealed a conserved PYIP (Pro79, Tyr80, Ile81, and Pro82) wedge motif on the protein surface (Dalhus et al., 2009). This conserved surface motif separates the two DNA strands and forms a physical barrier at one side of the lesion recognition pocket, into which the deaminated bases are flipped. The wedge motif was hypothesized to be crucial for the enzyme's ability to recognize DNA with helical distortions, such as base mismatches, ID loops, hairpins, flaps, and pseudo-Y structures.

DNA loops are predominantly formed by replication-associated strand slippage within repetitive sequences (Streisinger et al., 1966). Left unrepaired, these ID loops can lead to frameshift mutations if they occur within the open reading frame of a gene (Kunkel, 1990). Loops in DNA are normally recognized and removed by the mismatch repair (MMR) pathway in conjunction with DNA replication (reviewed in Iyer et al., 2006; Jiricny, 2006; Li, 2008). However, there is accumulating evidence suggesting that ID loops can also be removed by an alternative pathway distinct from the MMR system (Corrette-Bennett et al., 1999, 2001; Littman et al., 1999; Fang et al., 2003; McCulloch et al., 2003a, 2003b). In particular, a nick-directed loop repair has been detected in MMR-deficient cell extracts of *E. coli* (Littman et al., 1999; Fang et al., 2003). Human cells have also been shown to possess an MMR-independent means to incise DNA loops, apparently involving endonuclease(s) cleaving close to the ID loop, also on the complementary strand (McCulloch et al., 2003a). This endonucleolytic activity requires a pre-existing nick 3′ to the site of incision.

EndoV is suggested to have an important role in the repair of ID structures in DNA (Yao and Kow, 1996). To explain the molecular basis of EndoV-mediated recognition and incision of DNA loops, we solved the crystal structure of *Tma* EndoV in complex with DNA containing a one-nucleotide loop (A:TT). The structure reveals that the conserved PYIP motif is crucial for DNA loop recognition by physically separating the two

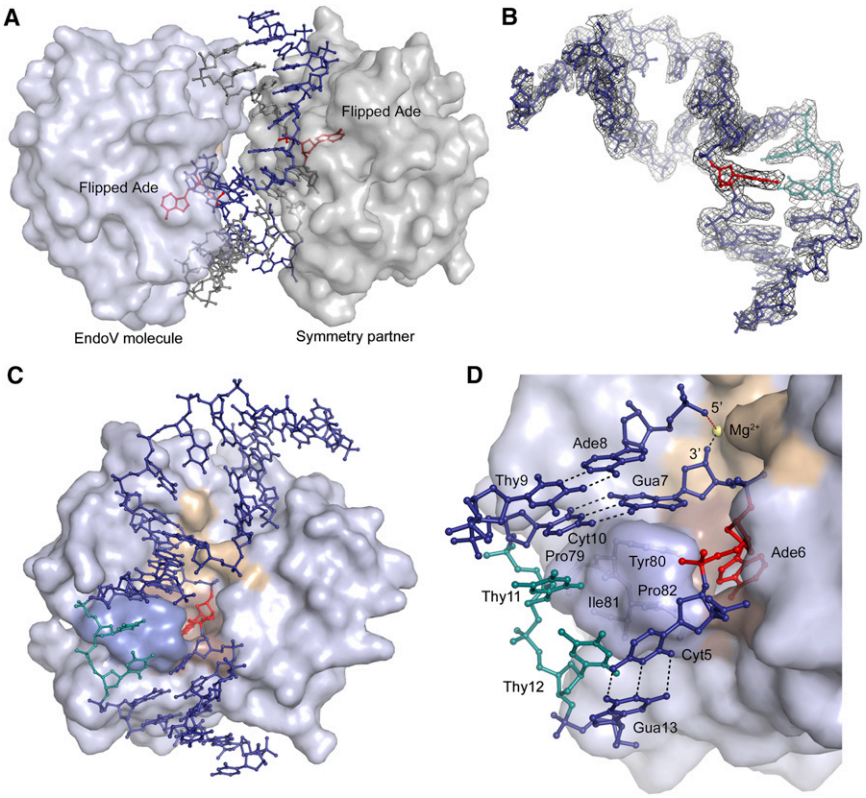

Figure 1. Crystal Structure of *Tma* EndoV in Complex with DNA Containing an A:TT Loop

(A) Crystal packing arrangement and protein-DNA complex formation. The double-stranded DNA is formed by oligomer self-annealing to give a duplex substrate with two symmetrical damages (ball-and-stick figures, red) binding two symmetrically related EndoV enzymes. Shown here is molecule B (in light blue) with its symmetry related partner (in gray) with bound DNA in corresponding colors. There are two such crystallographically independent dimeric entities in the crystal (molecule A with DNA is not shown here). Ade, adenine.

(B) $2f_o$-f_c electron density map for the DNA molecule contoured at the 1.0 σ level.

(C) Molecular surface representation of wild-type *Tma* EndoV bound to double-stranded DNA (ball-and-stick figures, dark blue) containing a TT loop (ball-and-stick figures, cyan) opposite an adenine (ball-and-stick figures, red). The DNA binding cleft of the protein contains three distinct regions: the conserved strand-separating PYIP motif (blue), the lesion recognition pocket (maroon) and the catalytic site (light pink).

(D) Close-up of the PYIP wedge motif that separates the two DNA strands at the loop. The PYIP residues (ball-and-stick figures, light blue) pushes the two thymine bases (cyan) in the loop partly out of the duplex, while the opposite adenine (red) is flipped into the lesion recognition pocket. The DNA bases on either side of the loop still have their hydrogen-bonding interactions intact (dashed lines, black) and remain paired. The active site Mg^{2+} interacts with the 3′ hydroxyl of Gua7 (dashed line, black) and with the 5′ phosphate of Ade8, probably via a bridging water molecule (dashed line, red). All structural display items are made using PyMOL (http://www.pymol.org).

mismatched strands. The additional loop-forming nucleotide rests on the surface of the wedge while the opposing adenine is inserted into the lesion recognition pocket, which normally recognizes the deaminated purine bases hypoxanthine and xanthine. The present complex structure reveals base flipping as a principle for DNA loop recognition. The shorter strand is cleaved at the second phosphodiester bond 3′ of the extrahelical adenine, with the 3′ and 5′ terminals held in place by a hydrogen bond network involving conserved residues in EndoV.

RESULTS

Structure Determination of *Tma* EndoV in Complex with a DNA Loop

To explore the molecular mechanism by which prokaryotic EndoV binds DNA loops, we determined the structure of wild-type *Tma* EndoV in complex with a self-annealing 17-mer DNA containing a symmetrically positioned one-nucleotide (A:TT) loop in each strand (Figure 1). The complex crystallized in space group *I*222, with two EndoV molecules binding to a double-stranded DNA formed by crystal symmetry (Figure 1A). There are two such crystallographically independent dimers in the crystal, with the asymmetric unit consisting of two halves of these dimeric particles combined. Inspection of the crystal packing reveals no substantial differences in protein contacts between the present DNA loop and the previously described hypoxanthine structures (Dalhus et al., 2009)—probably a key factor for obtaining crystals of EndoV binding to this weak loop substrate. Protein-protein crystal lattice contacts are confined to the ''backside'' of EndoV, away from the DNA binding surfaces surrounding the DNA duplex, and the DNA terminals at both ends of the duplex are not involved in crystal contacts. Diffraction data were collected to 2.75 Å resolution at the Berliner Elektronenspeicherring-Gesellschaft für Synchrotronstrahlung (BESSY) synchrotron in Berlin, Germany. The electron density of the sharply bent double-stranded DNA substrate (~60°) is well defined (Figure 1B), and nearly all bases could be included in the crystal structure model. The structure was refined by rigid body and simulated annealing refinement using phases from a modified version of 2W35 as input, and subsequently refined to final R_{work} and R_{free} factors of 0.23 and 0.29, respectively (Table 1).

The PYIP Motif Is Involved in DNA Loop Recognition

In the *Tma* EndoV-DNA loop complex, the protein binds the damaged DNA in a defined cleft consisting of the strand-separating PYIP motif, the lesion recognition pocket, and the active site (Figures 1C and 1D). The distorted helical DNA is recognized in a sequence-independent manner as the enzyme interacts with the sugar-phosphate backbone of the nonlooped DNA strand (Figure 2). Most of these polar protein-DNA interactions involve

Table 1. Summary of X-Ray Data Collection and Refinement Statistics for the *Tma* EndoV in Complex with Loop DNA

Data Collection	
Space group	*I*222
Unit cell dimensions	
a (Å)	55.23
b (Å)	135.37
c (Å)	194.99
Resolution range (Å)	58.62–2.75
Outer resolution shell (Å)	2.9–2.75
R_{sym}	0.13 (0.45)
Average $I/\sigma I$	10.6 (2.1)
Completeness (%)	99.1 (95.6)
Redundancy	3.9 (3.5)
Refinement	
Resolution (Å)	60–2.75
No. of reflections	17,361
R_{work}/R_{free}	0.23/0.29
No. atoms	
Protein	3580
Ligand/ion	631
Water	79
B factors	
Protein	42.6
Ligand/ion	75.1
Water	35.3
Root-Mean-Square Deviation	
Bond lengths (Å)	0.007
Bond angles (°)	1.35
Ramachandran Plot (%)[a]	
Preferred regions	92.0
Allowed regions	7.5
Disallowed regions	0.5

Values for outer-resolution shell are in parentheses.
[a]Calculated using Rampage in CCP4.

side chain atoms of the enzyme operating primarily at the 3′ side of the helical DNA distortion. Particularly important for DNA recognition is the aromatic side chain of Tyr80, which directly interacts with the phosphate group of the adenine opposite the TT loop (Figure 2). Additionally, this key residue is part of the conserved strand-separating PYIP wedge that is believed to work as a sensor recognizing various helical distortions in the DNA (Dalhus et al., 2009).

In this study, we observe that the PYIP wedge motif projects into the DNA minor groove at the loop distortion and leads to a local splitting of the two DNA strands. The two thymine bases in the loop are partly pushed out of the duplex, with Tyr80 filling the gap left by the opposite, flipped adenine. The wedge prevents formation of any polar interactions between nucleotides forming the loop and the corresponding flipped adenine partner; however, the Watson-Crick hydrogen bond patterns of the GC base pairs on either side of the loop remain intact (Figure 1D).

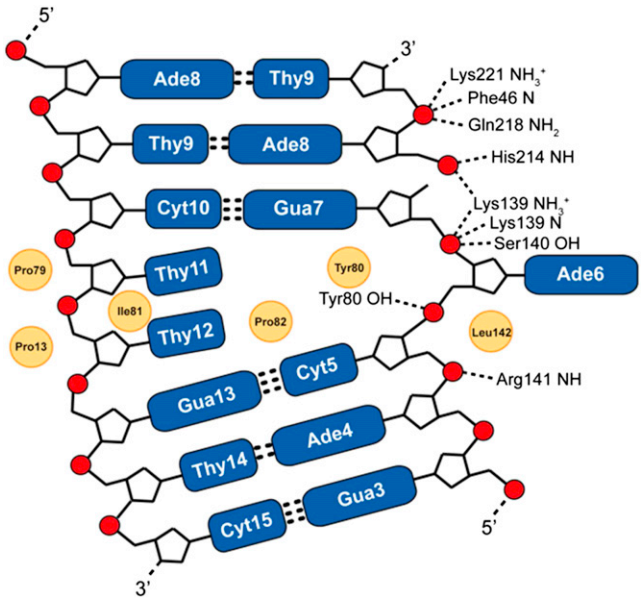

Figure 2. Protein-DNA Contacts in the Crystal Structure of *Tma* EndoV Binding to Loop DNA

Hydrogen bonding/ionic interactions (dashed lines) and steric interactions (orange circles) are shown for one of the two EndoV molecules binding symmetrically to the self-annealing DNA substrate containing a one-nucleotide A:TT loop. Most of the contacts occur at the 3′ side of the shorter strand containing the flipped adenine (Ade6). Only a part of the DNA on each side of the helical distortion is shown.

A Normal Adenine Is Inserted into the Lesion Recognition Pocket

The crystal structure reveals that the adenine base opposite the TT loop is rotated into a rigid lesion recognition pocket encircled with hydrophobic residues (Figure 3A). The polar protein interactions involved in base recognition predominantly include backbone atoms of the corresponding pocket residues. It is rather surprising that adenine is bound in the very same position and with the same orientation as its deaminated counterpart and main substrate, the hypoxanthine (Figure 3B). Adenine has a hydrogen bonding pattern similar to that of the tautomeric enol form of hypoxanthine, which is hypothesized to be the most favorable structural isomer with respect to the recognition pocket (Dalhus et al., 2009). Specifically, the amino group at the C6 position of adenine forms a hydrogen bond with the backbone carbonyl oxygen of Gly83, a residue that also interacts with the side chain of His116 (Figure 3A). The nonprotonated nitrogen atoms at adenine positions N1, N3, and N7 further ensure tight hydrogen binding to the backbone amide NH groups of Ile122, Gln112, and Gly83, respectively. In the structure of *Tma* EndoV binding to hypoxanthine, a solvent water molecule is also noticed interacting with the deaminated base. In the current structure at only 2.75Å resolution, no water molecule is observed in the vicinity of the recognition pocket; however, a corresponding interaction with adenine cannot be ruled out.

The DNA Strand Opposite the Loop Is Nicked

The structure presented here is that of the product complex, wherein the DNA substrate is nicked in the strand opposite of

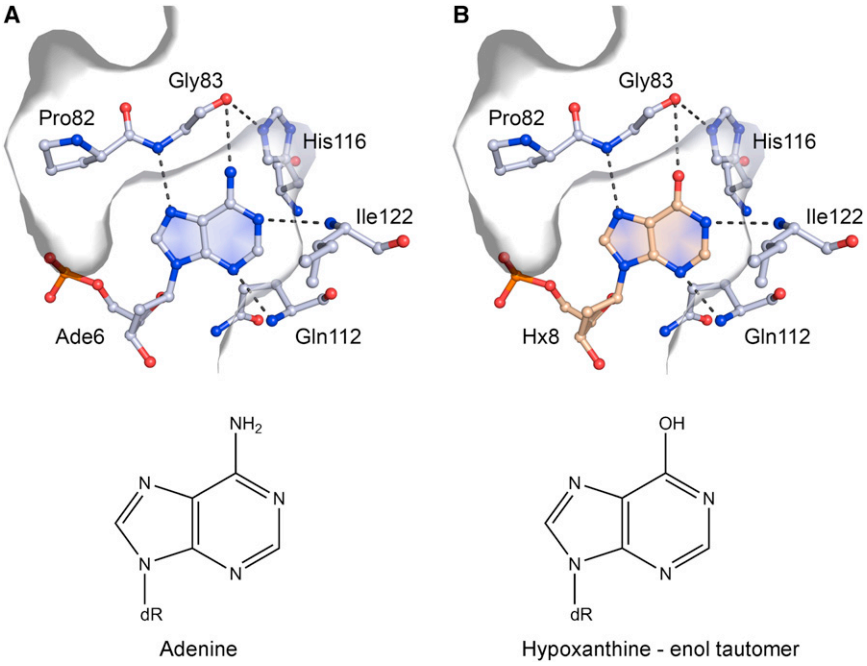

Figure 3. Comparison of the Lesion Binding Pockets of the Loop and Hypoxanthine Complexes

(A) The adenine (Ade6) in the loop substrate.

(B) The hypoxanthine (Hx8) in the deaminated substrate.

Ade6 in the loop substrate binds in the same position and with the same orientation as Hx8 in the deaminated substrate. In addition to the interactions shown, the carbonyl group in hypoxanthine also interacts with a solvent water molecule. A corresponding water molecule is not visible in the present 2.75 Å resolution of the loop structure in (A). The atomic coordinates for the hypoxanthine complex were retrieved from PDB entry 2W35. Assuming that the hypoxanthine base binds as an enol tautomer (Dalhus et al., 2009), the hydrogen bond interaction to Gly83 will be the same for these two bases.

the one-nucleotide loop. Similarly to hypoxanthine catalysis, EndoV hydrolyses the second phosphodiester bond 3′ of the flipped adenine, which can be observed as an unambiguous gap in the electron density map (Figure 4). The catalytically important Mg^{2+} ion is positioned between the 3′ OH group of Gua7 and the highly conserved residues Asp43 and Asp110. The active-site water molecules, coordinated to the metal ion and responsible for the hydrolytic activity, could not be detected at this resolution. Additionally, the free 5′ phosphate of Ade8 is firmly held in place by hydrogen bond interaction with the side chains of Lys139 and His214 (Figures 2 and 4). Lys139 also interacts with the DNA phosphate group on the 3′ side of the inserted adenine to further stabilize the nicked DNA product.

Tma EndoV Shows Weak but Significant Affinity and Activity for DNA Loops

The affinity of *Tma* EndoV for the A:TT loop was measured and compared with the canonical hypoxanthine substrate as well as undamaged DNA by electrophoretic mobility shift assay (EMSA). EMSA analysis showed only a weak affinity of *Tma* EndoV for the A:TT substrate, while *E. coli* EndoV clearly forms a strong complex with the DNA loop substrate (Figure 5A). The activity assay revealed a substantial endonucleolytic activity for the A:TT substrate, yet again with a much stronger effect for the *E. coli* homolog (Figure 5B).

Tma EndoV Binds A:TT Loops with Higher Affinity than Undamaged DNA

The equilibrium dissociation constant, K_D, for *Tma* EndoV-DNA complexes were determined for undamaged and A:TT loop-containing DNA substrates using surface plasmon resonance (SPR; Biacore) (Figure 6). Using the catalytically inactive D43A variant of *Tma* EndoV, K_D was determined for three different salt concentrations. As expected, the dissociation constant increases with increasing salt concentration in both series; however, the DNA loop substrate has an ~1.5- to 2-fold lower dissociation constant at the higher salt concentrations where unspecific DNA binding is expected to be less influential (Table 2). These SPR data are in agreement with the EMSA data (Figure 5A),

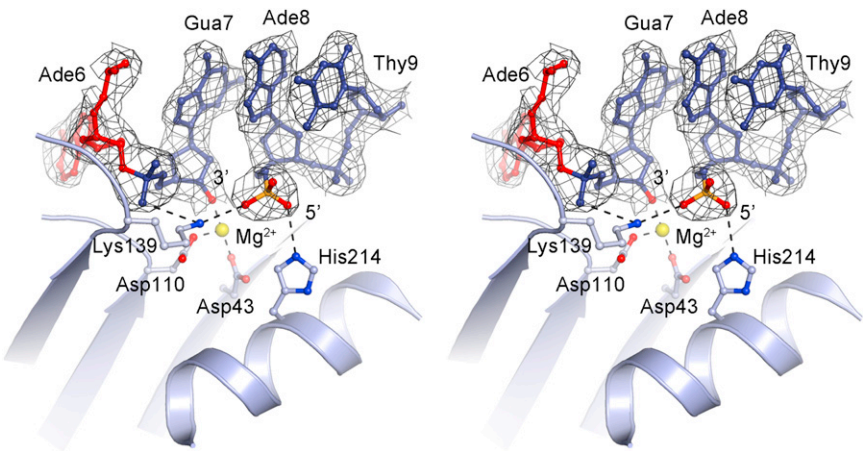

Figure 4. Cleavage of the DNA Strand Opposite the Loop

Stereo close-up view of the active site region of *Tma* EndoV showing the 3′ hydroxyl and the 5′ phosphate termini of the nicked substrate. A clear gap in the electron density (black mesh) is seen at the incision. The catalytically essential Mg^{2+} ion is shown as a yellow sphere interacting with the conserved Asp43 and Asp110 as well as the 3′ hydroxyl of Gua7. His214 coordinates with the 5′ phosphate, while Lys139 interacts with both the 5′ phosphate of the nick as well as the 3′ phosphate of Ade6.

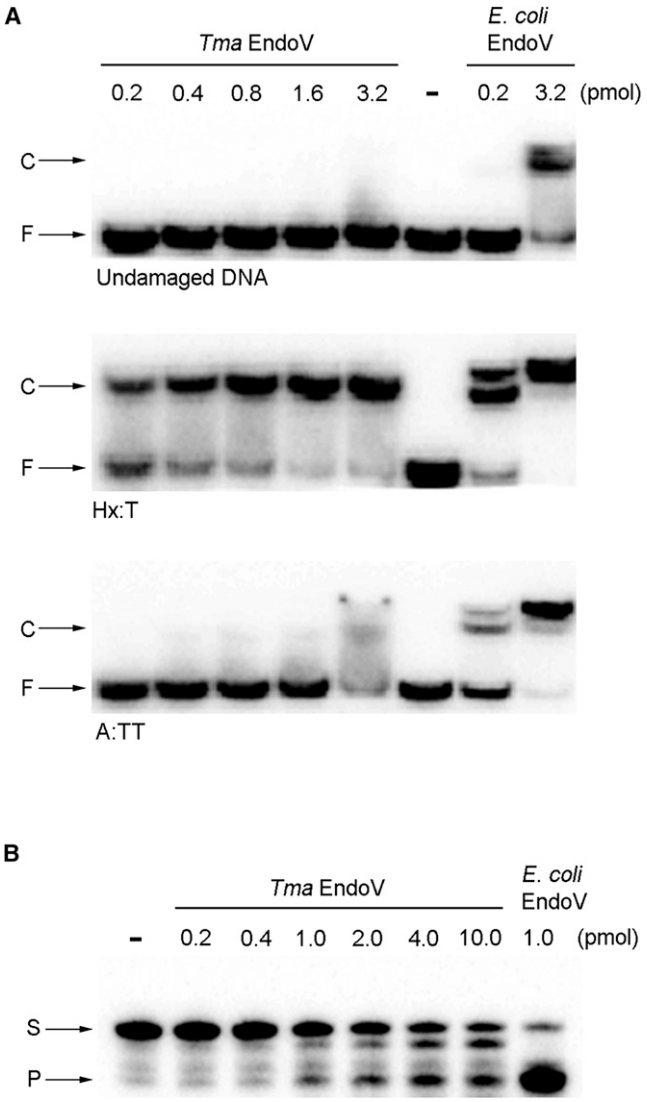

Figure 5. EMSA Binding and DNA Incision Activity Assay for *Tma* EndoV on DNA with Loop

(A) EMSA for D43A *Tma* EndoV binding to undamaged DNA, hypoxanthine in DNA (Hx:T), and loop DNA (A:TT). Duplex DNA (10 fmol) was incubated with *Tma* or *E. coli* EndoV as indicated for 15 min at 4°C before separation on 10% native PAGE. C, protein-DNA complex; F, free protein.

(B) DNA incision activity assay of wild-type *Tma* and *E. coli* EndoV for the A:TT loop substrate. DNA (10 fmol) was incubated with enzyme as indicated for 120 min at 50°C before separation on 20% PAGE. S, substrate; P, product.

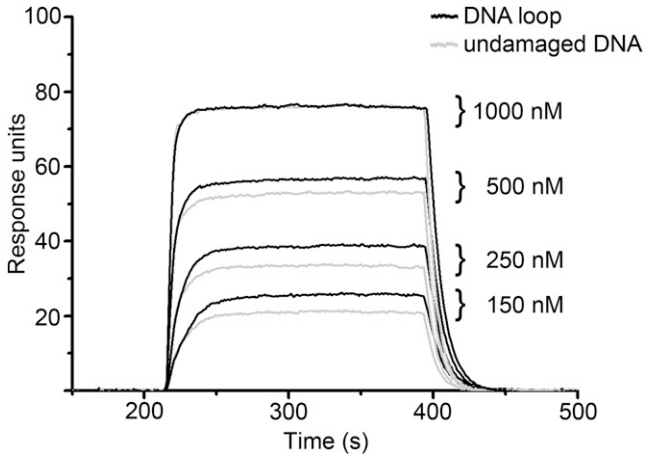

Figure 6. SPR Equilibrium Dissociation Constant Determination for Binding of Loop and Undamaged DNA by EndoV

Increasing amounts (150, 250, 500, and 1000 nM) of *Tma* EndoV (D43A mutant) were injected on a chip containing either undamaged DNA (light gray) or DNA with a one-nucleotide loop (black) for the experiment with 100 mM NaCl.

showing only a very weak affinity of *Tma* EndoV for the A:TT loop substrate. Nonetheless, rapid association of EndoV with the self-annealing DNA loop substrate may allow crystal nucleation of the protein-DNA complex in a dimeric form (Figure 1A), with crystal lattice interactions stabilizing the complex sufficient for growth and formation of crystals for structure determination.

DISCUSSION

ID loops in the DNA are generally repaired by the MMR system in order to avoid genomic instability caused by resulting frameshift mutations (Kunkel, 1990; Iyer et al., 2006; Jiricny, 2006; Li, 2008). However, previous studies demonstrate a DNA loop repair activity independent of MMR in *E. coli*, yeast, and human cell extracts (Corrette-Bennett et al., 1999, 2001; Littman et al., 1999; Fang et al., 2003; McCulloch et al., 2003a, 2003b). EndoV has been shown to recognize and catalyze DNA with helical distortions, including flaps and pseudo-Y structures, hairpins, and ID loops (Yao and Kow, 1996). This study reveals the underlying molecular mechanism of DNA loop recognition and complementary strand incision by EndoV at the atomic level.

The crystal structure of the EndoV-DNA loop complex reveals that the four-residue PYIP motif of the enzyme is important for the recognition of distortions in the DNA helix. Two thymine bases are partly pushed out of the helix, while the opposing single adenine is rotated by ~90° into the lesion recognition pocket (Figures 1C and 1D), normally accommodated by its deaminated analog, hypoxanthine (Figure 3). Binding affinity measurements by SPR (Table 2) and EMSA (Figure 5A) suggest that the DNA loop is a relatively weak substrate for EndoV. Since EndoV displays no activity for undamaged DNA, normal bases can consequently only be flipped into the recognition pocket when in the context of a helical DNA distortion. However, even with just one extra nucleotide present in one strand, as in the current DNA loop, the enzyme is able to detect this deviation from the normal base-stacking situation in the DNA helix, position the DNA in register with the active site, and flip a normal

Table 2. Equilibrium Dissociation Constants for the D43A Mutant of *Tma* EndoV Binding to Loop and Undamaged DNA as Determined by SPR

	K_D (μM) ± SD for Salt Concentrations		
Substrate	50 mM	100 mM	150 mM
Undamaged DNA	0.11 ± 0.03	0.92 ± 0.07	7.5 ± 0.2
1 nucleotide loop DNA	0.11 ± 0.01	0.66 ± 0.03	3.7 ± 0.1

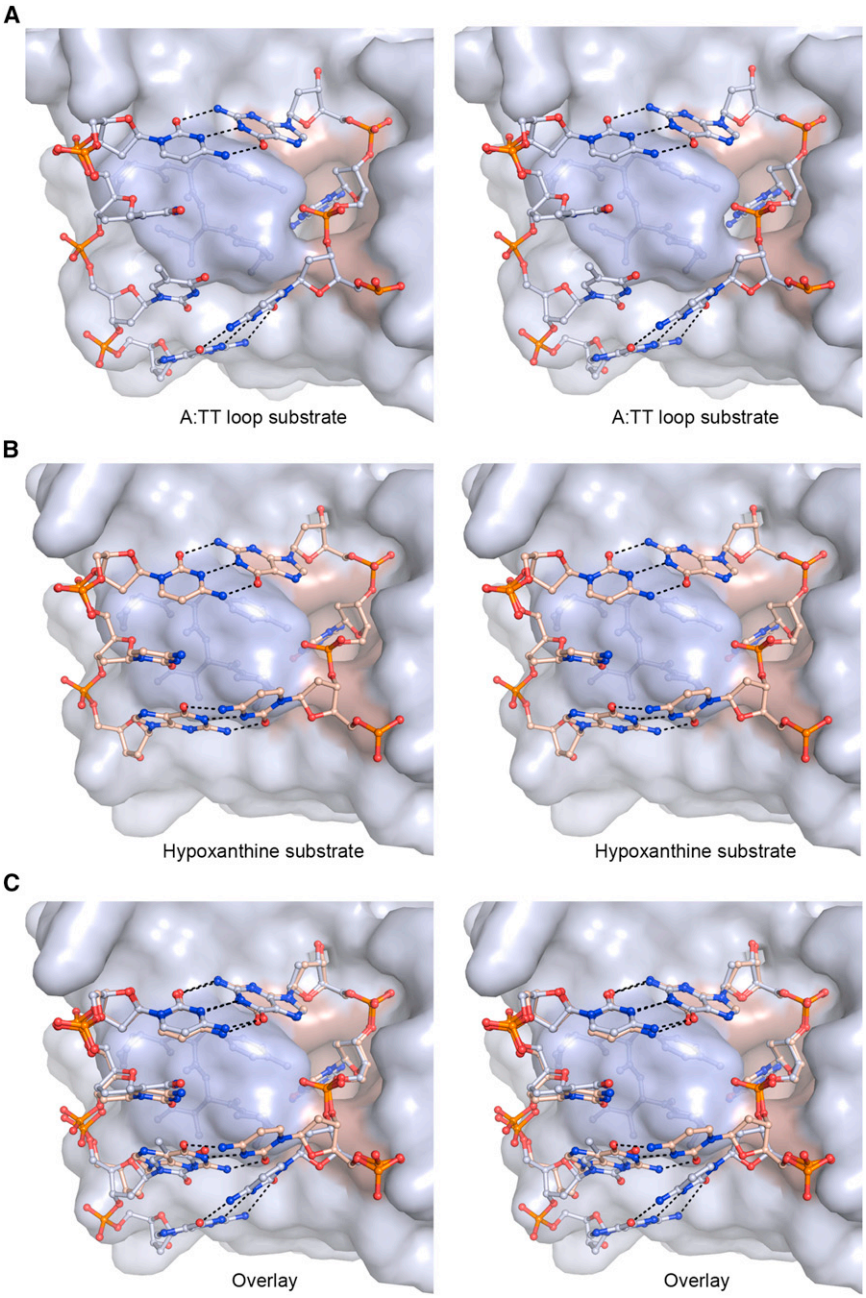

Figure 7. DNA Wrapping around the Strand-Separating Wedge

(A) Stereo close-up view of the wedge region in the loop substrate. The two unpaired thymine bases rest on the surface of the wedge.

(B) Stereo close-up view of the wedge region in the hypoxanthine (Hx) substrate. The unpaired base opposite Hx rests on the surface of the wedge.

(C) Stereo close-up view of a superposition of the loop substrate in (A) and the hypoxanthine substrate in (B) showing the adjustments in DNA conformation to accommodate the additional thymine in the loop substrate.

nucleotide into the preformed pocket (Figure 3A). The DNA strand containing the short loop passes around the wedge (Figures 1C and 1D). Comparison of the DNA contacts in the wedge area between the A:TT loop substrate and the canonical hypoxanthine substrate shows only minor differences in positions of the nucleotides (Figure 7). The extra thymine in the loop is not involved in base-specific interactions with the protein (Figure 7A). The G:C base pair on the 5′ side of the flipped adenine in the loop complex (Figure 7A) is shifted by a few angstroms relative to the hypoxanthine substrate (Figure 7B) to accommodate the extra thymine nucleotide in the loop-containing strand.

The affinity of *Tma* EndoV for the A:TT loop substrate is, however, much weaker than the main substrate, hypoxanthine. Even though the normal adenine has the same orientation and position as hypoxanthine within the recognition pocket (Figure 3), the reduced binding affinity (Figure 5A) and incision activity demonstrates that DNA binding and incision is clearly optimized for the deaminated counterpart. The carbonyl oxygen of residue Gly83 thus appears to be involved in discrimination between the oxidized enolic hydroxyl of hypoxanthine and the amine group at the C6 position of adenine. However, the present structure shows that also normal adenine may be accommodated in the lesion binding pocket. Since EndoV neither binds nor cleaves A:T base pairs in normal DNA, the difference in affinity between native DNA and the DNA loop substrate must reside with the extra nucleotide resting on the surface of the strand-separating wedge, combined with the insertion of a suboptimal nucleotide flipped into the binding pocket allowed by an inherent weak point in the DNA.

Given the fact that *Tma* EndoV exhibits no direct and specific contacts with the bases but predominately interacts with the sugar-phosphate backbone of the DNA substrate, EndoV displays a sequence-independent detection of damage. This feature is also true for the DNA repair enzyme DDB2, which is part of the UV-damage DNA-binding protein complex operating in the nucleotide excision repair pathway (Scrima et al., 2008; Schärer and Campbell, 2009). DDB2 also uses a wedge-like mechanism to probe for DNA lesions, through the insertion of a strictly conserved hairpin wedge (Phe371, Gln372, and His373) into the minor groove of DNA. Moreover, DDB2 provides only modest specificity for the (6-4) photoproduct and also binds various lesions with an intrastrand crosslink such as cyclopyrimidine dimers. Considering the similarity in using a wedge motif as

a damage sensor in these unrelated DNA repair enzymes, it would be of great interest to investigate the DNA scanning characteristic of EndoV and DDB2 in more detail, particularly the roles of these wedges as DNA-groove and damage-detection sensors.

In eukaryotes and most bacteria, repair of mismatches and ID loops by the MMR pathway is directed to the newly synthesized strand by the recognition of a pre-existing strand break (reviewed in Li, 2008; Fukui, 2010). Likewise, the *E. coli* MMR system exploits hemimethylated GATC sites as a signal for strand discrimination (Längle-Rouault et al., 1987; Lahue and Modrich, 1988; Modrich, 1989). The structure presented here reveals that EndoV cleaves the shorter strand, in agreement with previously published studies (Yao and Kow, 1996). Since EndoV incises the shorter strand opposite the loop, detrimental frameshift mutations could, in fact, be introduced by EndoV. Analogous, recent work has shown that human DNA glycosylases can induce genomic instability and frameshift mutagenesis upon DNA loop recognition (Klapacz et al., 2010; Lyons and O'Brien, 2010). Human AAG was shown to bind DNA containing one- and two-nucleotide loops, thereby shielding them from the MMR machinery. Specifically, an increase in spontaneous frameshift mutations was detected in cells overexpressing AAG (Klapacz et al., 2010).

Studies in *E. coli* and human cells have discovered a nick-directed DNA loop repair activity that is distinct from the MMR pathway (Littman et al., 1999; Fang et al., 2003; McCulloch et al., 2003a, 2003b). In *E. coli* extracts, this activity requires Mg^{2+} and the four dNTPs (Fang et al., 2003). Furthermore, this MMR-independent activity in human cell extracts seems to involve endonuclease(s) cleaving also the complementary strand close to the loop. This endonucleolytic activity depends on a pre-existing nick located on the 3′ side of the site of incision (McCulloch et al., 2003a). In this respect, it would be interesting to explore whether EndoV could be involved in an MMR-independent DNA loop incision activity, since EndoV both uses Mg^{2+} as a cofactor and incises the shorter DNA strand close to the loop. If this is the case, DNA loop incision activity by EndoV will lead to frameshift mutations or genomic restoration for insertion loops or deletion loops, respectively.

EXPERIMENTAL PROCEDURES

Protein Expression, Purification, and Crystallization

Cells containing plasmids of the full-length sequences of wild-type and D43A *Tma* EndoV were incubated in Luria broth medium supplemented with 50 μg ml^{-1} kanamycin at 37°C. Protein expression was induced by adding 0.5 mM IPTG at optical density 600 (OD_{600}) of ~0.75, followed by overnight incubation at 18°C. Cells were harvested by centrifugation and resuspended in buffer A (50 mM NaCl, 20 mM MES, pH 6.5, and 10 mM β-mercaptoethanol [β-ME]) supplemented with 0.3 mg ml^{-1} DNase I (Roche). Cells were disrupted by sonication and centrifuged at 27,000 × g for 30 min. The protein extracts were incubated at 75°C for 15 min followed by a second centrifugation step. The supernatants were loaded on to a 5 ml HiTrap SP XL column (GE Healthcare) equilibrated with buffer A. The protein was eluted using a linear salt gradient to 1 M NaCl in buffer A. Fractions rich in *Tma* EndoV were pooled, concentrated, and further purified by size exclusion chromatography (Superdex 75) with concomitant buffer exchange (100 mM NaCl, 20 mM MES, pH 6.5, and 10 mM β-ME). Protein fractions containing *Tma* EndoV were pooled, concentrated, and stored at −20°C. A 17-mer self-annealing DNA oligonucleotide (Eurofins MWG/Operon) with sequence 5′-GCGACAGATCTTGTCGC-3′ was dissolved in water and annealed by heating to 80°C for 2 min before slow cooling to form a double-stranded DNA containing two loops. Purified wild-type *Tma* EndoV at a concentration of 8.5 mg/ml was supplemented with 5 mM $MgCl_2$ for >15 min on ice. The DNA loop substrate was added to the protein in a 1.5:1 stoichiometric ratio, and the mixture was equilibrated for >30 min on ice. Diamond-shaped crystals of the complex were obtained by vapor diffusion at room temperature using hanging drops equilibrated against 15% polyethylene glycol (PEG 400) and 100 mM MES, pH 6.25. Crystals were cryoprotected by a short soak in 30% PEG 400 and 100 mM MES, pH 6.5, followed by flash freezing in liquid nitrogen prior to data collection.

X-Ray Diffraction Data Collection, Structure Determination, and Refinement

Diffraction data to 2.75 Å resolution (T = 100 K, λ = 0.9184 Å) were collected at beamline 14.1 at BESSY (Berlin, Germany). The data set was processed using MOSFLM (Battye et al., 2011), and the integrated data were scaled and merged using CCP4/Scala (Collaborative Computational Project, Number 4, 1994). The loop complex crystallized in the same space group as the hypoxanthine complex (*I*222), and the structure was determined by rigid body and simulated annealing refinement in CNS 1.1 (Brünger et al., 1998), using initial phases from the protein part of the wild-type EndoV structure (Protein Data Bank [PDB] ID 2W35). Manual model building of the DNA and addition of solvent molecules were performed using Coot (Emsley and Cowtan, 2004), and the improvement of the model was monitored by a steady decrease in R_{free} during the refinement. The asymmetric unit contains two separate EndoV molecules, each binding to a single-stranded DNA. Via 2-fold crystal symmetry, each EndoV-DNA complex in the asymmetric unit forms duplex DNA containing two DNA loops binding to their respective EndoV molecules. Crystal data, data collection, and refinement statistics are summarized in Table 1.

SPR Sensorgram Acquisition

SPR measurements were performed using a Biacore 3000 system (Biacore Inc., Uppsala, Sweden). Prior to DNA immobilization, the SA sensor chip was conditioned with three consecutive 1-min injections of 50 mM NaOH in 1M NaCl. Fifteen micromolar single-stranded DNA oligomers containing either +1 nucleotide loop (loop oligo; 5′-CGAGTACGGCAGTTCTCGCTAG AAG-3′) or no damage (undamaged oligo; (5′-CGAGTACGGCAGTCTCGCTA GAAG-3′) were slowly annealed with 5 μM complementary oligomer with a 5′ biotin tag (complementary oligo; 5′biotin-CTTCTAGCGAGACTGCCGTA CTCG-3′). The double-stranded ligands were diluted to a concentration of 10 nM and immobilized on the SA chip to a level of 60–65 resonance units. Concentrations from 150 nM to 2 μM, 4 μM, or 16 μM (depending on the concentration of NaCl in the running buffer, respectively) of the catalytically inactive *Tma* EndoV D43A mutant were injected using the Kinject function (50 μl/min, 25°C) with a 180 s association phase followed by a 300 s flow of running buffer for the dissociation phase. Three different running buffers were used containing 10 mM Tris, pH 7.5, 5 mM $MgCl_2$, 0.005% Surfactant P20, and 50, 100, or 150 mM NaCl, respectively. Equilibrium dissociation constants, K_D, were obtained by plotting the responses at equilibrium versus enzyme concentration, followed by fitting of the steady-state affinity model.

Oligonucleotides and [^{32}P] Labeling

The DNA substrates for electrophoretic mobility shift assay (EMSA) and DNA nicking activity measurements were prepared by 5′ end labeling of the same oligonucleotides as for the SPR experiments (minus the 5′ biotin tag) using T4 polynucleotide kinase (New England BioLabs, Hitchin, UK) in the presence of [γ-^{32}P]ATP (Amersham Biosciences). The radioactively labeled oligomers (the Hx oligo for Hx:T and the complementary oligo for the loop and undamaged substrates) were annealed to their respective complementary strands by heating the solution to 90°C for 2 min and slowly cooling to room temperature. The double-stranded substrates were separated by 10% native PAGE, excised from the gel, eluted by diffusion in H_2O, and stored at 4°C.

EMSA

The binding affinity of *Tma* EndoV for A:TT loop, Hx:T and undamaged DNA substrates was analyzed by EMSA. Ten fmol of each DNA substrate was

mixed with an increasing amount of enzyme (0.2–3.2 pmol) and incubated in a 10 μl reaction volume (5 mM $CaCl_2$, 10 mM HEPES-KOH, pH 7.4, 1 mM dithiothreitol [DTT], and 20% glycerol) at 4°C for 15 min. DNA loading buffer (Fermentas) was added, and the samples were separated by 10% native PAGE (Long Ranger, 1× taurin, 5 mM $CaCl_2$) on ice. Results were visualized by phosphorimaging and quantified with ImageQuant TL software. *E. coli* EndoV was used as a positive control.

DNA Nicking Activity

Various amounts (0.2–10 pmol) of *Tma* EndoV were mixed with 10 fmol substrate DNA and reaction buffer (10 mM Tris-HCl, pH 8.5, 0.34 mM $MnCl_2$, 50 mM KCl, 5% glycerol, and 1 mM DTT) in a total volume of 10 μl and incubated at 50°C for 120 min. The reactions were stopped by adding formamide loading buffer (80% formamide, 10 mM EDTA, and bromphenol blue) and heating to 85°C for 3 min. Cleavage products were analyzed by 20% PAGE (Long Ranger, 7 M urea, 1× taurin), visualized by phosphorimaging, and quantified by ImageQuant TL. *E. coli* EndoV was used as a positive control.

ACCESSION NUMBERS

Atomic coordinates and structure factors have been deposited in the Protein Data Bank with accession code 4B20.

ACKNOWLEDGMENTS

We thank the staff at beamline 14.1 at BESSY for assistance with data collection and Ellen Cecilie Gustad and Meh Sameen Nawaz for technical assistance.

E.S.V., I.A., and B.D. have received support from the Norwegian Cancer Society and the MLS^{UiO} program for Molecular Life Science research at the University of Oslo. M.B. was supported by the Research Council of Norway and the Norwegian Cancer Society. B.D. and M.B. were also supported by the South-Eastern Norway Regional Health Authority (Grants 2009100 and 2011040) for establishing the Regional Core Facility for Structural Biology and Bioinformatics.

Received: July 6, 2012
Revised: November 19, 2012
Accepted: December 2, 2012
Published: January 10, 2013

REFERENCES

Battye, T.G.G., Kontogiannis, L., Johnson, O., Powell, H.R., and Leslie, A.G.W. (2011). iMOSFLM: a new graphical interface for diffraction-image processing with MOSFLM. Acta Crystallogr. D Biol. Crystallogr. *67*, 271–281.

Brünger, A.T., Adams, P.D., Clore, G.M., DeLano, W.L., Gros, P., Grosse-Kunstleve, R.W., Jiang, J.S., Kuszewski, J., Nilges, M., Pannu, N.S., et al. (1998). Crystallography & NMR system: A new software suite for macromolecular structure determination. Acta Crystallogr. D Biol. Crystallogr. *54*, 905–921.

Collaborative Computational Project, Number 4. (1994). The CCP4 suite: programs for protein crystallography. Acta Crystallogr. D Biol. Crystallogr. *50*, 760–763.

Corrette-Bennett, S.E., Parker, B.O., Mohlman, N.L., and Lahue, R.S. (1999). Correction of large mispaired DNA loops by extracts of Saccharomyces cerevisiae. J. Biol. Chem. *274*, 17605–17611.

Corrette-Bennett, S.E., Mohlman, N.L., Rosado, Z., Miret, J.J., Hess, P.M., Parker, B.O., and Lahue, R.S. (2001). Efficient repair of large DNA loops in Saccharomyces cerevisiae. Nucleic Acids Res. *29*, 4134–4143.

Dalhus, B., Arvai, A.S., Rosnes, I., Olsen, Ø.E., Backe, P.H., Alseth, I., Gao, H., Cao, W., Tainer, J.A., and Bjørås, M. (2009). Structures of endonuclease V with DNA reveal initiation of deaminated adenine repair. Nat. Struct. Mol. Biol. *16*, 138–143.

Demple, B., and Linn, S. (1982). On the recognition and cleavage mechanism of Escherichia coli endodeoxyribonuclease V, a possible DNA repair enzyme. J. Biol. Chem. *257*, 2848–2855.

Emsley, P., and Cowtan, K. (2004). Coot: model-building tools for molecular graphics. Acta Crystallogr. D Biol. Crystallogr. *60*, 2126–2132.

Fang, W.H., Wang, B.-J., Wang, C.-H., Lee, S.-J., Chang, Y.-T., Chuang, Y.-K., and Lee, C.-N. (2003). DNA loop repair by Escherichia coli cell extracts. J. Biol. Chem. *278*, 22446–22452.

Fladeby, C., Vik, E.S., Laerdahl, J.K., Gran Neurauter, C., Heggelund, J.E., Thorgaard, E., Strøm-Andersen, P., Bjørås, M., Dalhus, B., and Alseth, I. (2012). The human homolog of Escherichia coli endonuclease V is a nucleolar protein with affinity for branched DNA structures. PLoS ONE *7*, e47466.

Friedberg, E.C., Walker, G.C., and Siede, W. (2006). DNA Repair and Mutagenesis (Washington, DC: ASM Press).

Fukui, K. (2010). DNA Mismatch Repair in Eukaryotes and Bacteria. J. Nucleic Acids *2010*, 239–240.

Hitchcock, T.M., Gao, H., and Cao, W. (2004). Cleavage of deoxyoxanosine-containing oligodeoxyribonucleotides by bacterial endonuclease V. Nucleic Acids Res. *32*, 4071–4080.

Hoeijmakers, J.H. (2001). Genome maintenance mechanisms for preventing cancer. Nature *411*, 366–374.

Hoeijmakers, J.H. (2009). DNA damage, aging, and cancer. N. Engl. J. Med. *361*, 1475–1485.

Huang, J., Lu, J., Barany, F., and Cao, W. (2001). Multiple cleavage activities of endonuclease V from Thermotoga maritima: recognition and strand nicking mechanism. Biochemistry *40*, 8738–8748.

Iyer, R.R., Pluciennik, A., Burdett, V., and Modrich, P.L. (2006). DNA mismatch repair: functions and mechanisms. Chem. Rev. *106*, 302–323.

Jiricny, J. (2006). The multifaceted mismatch-repair system. Nat. Rev. Mol. Cell Biol. *7*, 335–346.

Klapacz, J., Lingaraju, G.M., Guo, H.H., Shah, D., Moar-Shoshani, A., Loeb, L.A., and Samson, L.D. (2010). Frameshift mutagenesis and microsatellite instability induced by human alkyladenine DNA glycosylase. Mol. Cell *37*, 843–853.

Kunkel, T.A. (1990). Misalignment-mediated DNA synthesis errors. Biochemistry *29*, 8003–8011.

Lahue, R.S., and Modrich, P. (1988). Methyl-directed DNA mismatch repair in Escherichia coli. Mutat. Res. *198*, 37–43.

Li, G.-M. (2008). Mechanisms and functions of DNA mismatch repair. Cell Res. *18*, 85–98.

Lindahl, T. (1993). Instability and decay of the primary structure of DNA. Nature *362*, 709–715.

Littman, S.J., Fang, W.H., and Modrich, P. (1999). Repair of large insertion/deletion heterologies in human nuclear extracts is directed by a 5′ single-strand break and is independent of the mismatch repair system. J. Biol. Chem. *274*, 7474–7481.

Lyons, D.M., and O'Brien, P.J. (2010). Human Base Excision Repair Creates a Bias Toward −1 Frameshift Mutations. J. Biol. Chem. *285*, 25203–25212.

Längle-Rouault, F., Maenhaut-Michel, G., and Radman, M. (1987). GATC sequences, DNA nicks and the MutH function in Escherichia coli mismatch repair. EMBO J. *6*, 1121–1127.

McCulloch, S.D., Gu, L., and Li, G.-M. (2003a). Bi-directional processing of DNA loops by mismatch repair-dependent and -independent pathways in human cells. J. Biol. Chem. *278*, 3891–3896.

McCulloch, S.D., Gu, L., and Li, G.-M. (2003b). Nick-dependent and -independent processing of large DNA loops in human cells. J. Biol. Chem. *278*, 50803–50809.

Modrich, P. (1989). Methyl-directed DNA mismatch correction. J. Biol. Chem. *264*, 6597–6600.

Schärer, O.D., and Campbell, A.J. (2009). Wedging out DNA damage. Nat. Struct. Mol. Biol. *16*, 102–104.

Scrima, A., Konícková, R., Czyzewski, B.K., Kawasaki, Y., Jeffrey, P.D., Groisman, R., Nakatani, Y., Iwai, S., Pavletich, N.P., and Thomä, N.H.

(2008). Structural basis of UV DNA-damage recognition by the DDB1-DDB2 complex. Cell *135*, 1213–1223.

Streisinger, G., Okada, Y., Emrich, J., Newton, J., Tsugita, A., Terzaghi, E., and Inouye, M. (1966). Frameshift mutations and the genetic code. Cold Spring Harb. Symp. Quant. Biol. *31*, 77–84.

Weiss, B. (2008). Removal of deoxyinosine from the Escherichia coli chromosome as studied by oligonucleotide transformation. DNA Repair (Amst.) *7*, 205–212.

Yao, M., and Kow, Y.W. (1994). Strand-specific Cleavage of Mismatch-containing DNA by Deoxyinosine 3′-Endonuclease from Escherichia coli. J. Biol. Chem. *269*, 31390–31396.

Yao, M., and Kow, Y.W. (1995). Interaction of deoxyinosine 3′-endonuclease from Escherichia coli with DNA containing deoxyinosine. J. Biol. Chem. *270*, 28609–28616.

Yao, M., and Kow, Y.W. (1996). Cleavage of insertion/deletion mismatches, flap and pseudo-Y DNA structures by deoxyinosine 3′-endonuclease from Escherichia coli. J. Biol. Chem. *271*, 30672–30676.

Yao, M., and Kow, Y.W. (1997). Further characterization of Escherichia coli endonuclease V. Mechanism of recognition for deoxyinosine, deoxyuridine, and base mismatches in DNA. J. Biol. Chem. *272*, 30774–30779.

Yao, M., Hatahet, Z., Melamede, R.J., and Kow, Y.W. (1994). Purification and characterization of a novel deoxyinosine-specific enzyme, deoxyinosine 3′ endonuclease, from Escherichia coli. J. Biol. Chem. *269*, 16260–16268.

